PAPER

www.rsc.org/loc

# Total internal reflection-based biochip utilizing a polymer-filled cavity with a micromirror sidewall

**Nikolas Chronis and Luke P. Lee***

*Berkeley Sensor and Actuator Center, Department of Bioengineering, University of California, Berkeley, USA. E-mail: lplee@socrates.berkeley.edu; Fax: 510-6436637; Tel: 510-6433389*

***Received 11th September 2003, Accepted 30th January 2004***
***First published as an Advance Article on the web 17th February 2004***

A total internal reflection (TIR)-based biochip utilizing a polymer-filled cavity with a micromirror sidewall has been designed and fabricated. The implementation of the micromirror sidewall cavity facilitates precise alignment of the excitation light beam into the system. The incident angle of illumination can be easily modified by selecting polymers of different indices of refraction while optical losses are minimized. The design enables the hybrid, vertical integration of a laser diode and a CCD camera, resulting in a compact optical system. Brownian motion of fluorescent microspheres and real-time photobleaching of rhodamine 6G molecules is demonstrated. The proposed TIR-based chip simplifies current TIR optical configurations and could potentially be used as an optical-microfluidic platform for an integrated lab-on-a-chip microsystem.

## A Introduction

Among the various systems used for optically, electronically or mechanically sensing/imaging biological samples,[1] those that can identify changes in optical properties, especially fluorescence, are the most popular, with applications ranging from cell imaging to monitoring gene expression in DNA microarrays to even single molecule detection. Wide field epi-fluorescence microscopy, confocal microscopy and total internal reflection fluorescence microscopy (TIRFM) are techniques routinely used for such purposes.

In particular, TIRFM, also known as evanescent wave microscopy, has received considerable recognition in recent years due to its unique capabilities. TIRFM enables the study of surface molecular dynamics at the single molecule level through the generation of a thin evanescent wave at a glass/liquid interface by total internal reflection (TIR). TIRM has been successfully utilized in detecting real-time DNA surface attachment and hybridization[2,3] and recording molecular motors activity.[4]

The distinctive advantages of TIRFM in applications where confined fluorescence excitation near a solid surface is desired, combined with the design simplicity of most of the optical configurations employing TIR,[5] motivated the design of miniaturized evanescent excitation-based optical systems. Such systems can be components of major importance for the further development of integrated advanced micro total analysis systems (μTAS) with a capability of massively-parallel processing for high throughput screening.

Based on TIR, disposable plastic prisms integrated on biochips[6] and various types of evanescent waveguides including fibers[7] channel[8] and planar waveguides[9,10] have been proposed to address the requirements for ultra-sensitive, high-throughput platforms. In all these systems, the excitation laser beam, coming from the side of the chip, must be aligned at a certain angle to achieve efficient light coupling and to create a strong evanescent field. Such optical configuration is unsuitable for the development of a fully integrated miniaturized system, since it requires the precise alignment of tilted optical components into the chip.

Moreover, the fabrication of high refractive index waveguides and short-period gratings requires the use of special equipment, which in turn greatly increases the cost of the chip. Gratings and waveguides also suffer from light coupling and propagation losses. These limitations can only be overcome with the use of bulky, high power, expensive lasers. Plastic prisms on the other hand can be inexpensively fabricated, but their use in an array-type format for high throughput processing is still questionable.

Our effort is focused on designing a TIR-based biochip platform (Fig. 1) that simplifies current TIR configurations and fabrication processes while providing flexibility for the future development of an integrated miniaturized optical system.

The biochip consists of a polymer-filled cavity for efficient light coupling. One of the reflective sidewalls of the cavity act as a micromirror that directs the excitation light at a predefined angle. Microfluidic channels are also integrated on top of the chip for sample delivery.

The chip is fabricated using a combination of standard bulk micromachining techniques and PDMS casting. It enables the hybrid vertical integration of all of the optical components, providing great design flexibility for future miniaturization. The design can potentially incorporate hundreds of detection sites on a single chip, suiting it for various array-type bioassays. In such a configuration the chip would be scanned with respect to a stationary excitation–detection system.

## B Theoretical background

TIR takes place when light travels from a high (*e.g.* glass coverslip, index of refraction $n_1 = 1.52$) to a lower (*e.g.* water, cells, index of refraction $n_2 = 1.33$–$1.38$) refractive index medium at an incident angle above the critical angle ($\theta_C = \sin^{-1}(n)$, where $n = n_2/n_1$).

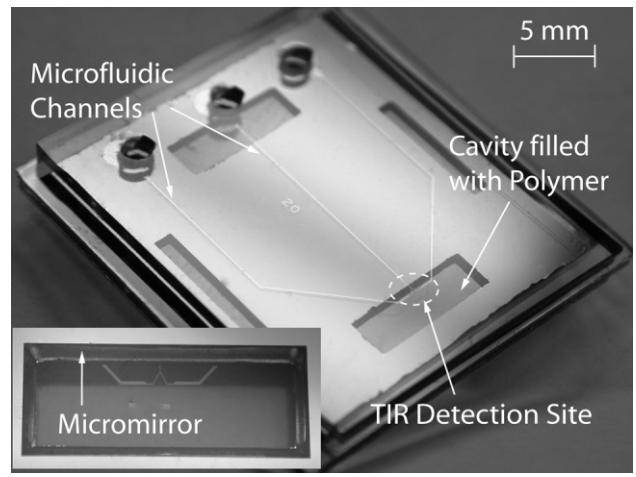


**Fig. 1** The TIR-based biochip with integrated microfluidic channels forming a Y configuration. Four cavities are shown with one that is active (where the channels cross). The backside of the chip is shown in the inset.

DOI: 10.1039/b311088e

The light is reflected at the interface and an evanescent component, which decays exponentially with distance, exists near the surface of the lower refractive index media. The selective excitation of fluorophores located only within the evanescent electromagnetic field (generally less than 200 nm) results in high signal to noise ratio fluorescence enabling the detection of even single fluorescent molecules.

For a weakly focused beam of wavelength $\lambda$, the intensity of the evanescent field $I(z)$ (measured in units of energy per unit area per second) as a function of the distance $z$ from the interface, can be calculated from:[11]

$$I(z) = I(0)e^{-z/d}$$
$$d = \frac{\lambda}{4\pi}\left(n_1^2 \sin^2\theta - n_2^2\right)^{-1/2} \quad (1)$$

where $I(0)$, the intensity of the evanescent wave at the interface ($z = 0$), depends on the two indices of refraction $n_1$ and $n_2$, the incident angle of illumination $\theta$ and the polarization of the incident light. The p-polarized (parallel to the plane of incidence) and s-polarized (perpendicular to the plane of incidence) components of $I(0)$ are given by:

$$I_p(0) = |A_p|^2 \frac{\left(4\cos^2\theta\right)\left(2\sin^2\theta - n^2\right)}{n^4\cos^2\theta + \sin^2\theta - n^2}$$
$$I_s(0) = |A_s|^2 \frac{4\cos^2\theta}{1-n^2} \quad (2)$$

where $A_P$ and $A_S$ are the corresponding p-polarized and s-polarized incident electric fields amplitudes at the interface. Operation near the critical angle assures strong evanescent intensity. Proper selection of the angle $\theta$ is therefore a key feature when designing TIR optical configurations.

## C Chip design and fabrication

Fig. 2 shows a schematic cross section of the chip and the path of the light beam as it passes through. A polymer-filled cavity and its micromirror sidewall are implemented to direct the excitation light beam at an angle above the critical angle on the glass–liquid interface. The geometry of such a micromirror makes it possible to vertically integrate a light source directly below the micromirror with no need of any external optics. More importantly, this design eliminates the need to align the light beam into the system at the desired angle. The angle of the tilted micromirror is accurately defined by the microfabrication process (54.7 ° for standard KOH etch of a {100} silicon wafer) and it can be changed by properly selecting polymers of different index of refraction (see section E). Dynamically changing the incident angle[12] is not an advantageous feature for lab-on-a-chip applications, since it requires the use of a complex optical and mechanical configuration and the interaction of the end-user with the system.

The chip consists of four substrates stacked together. A silicon substrate that contains the micromirror, sits between two thin

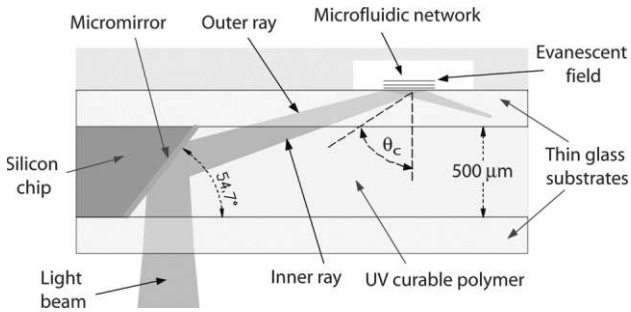


**Fig. 2** Schematic cross-section of the four-layer chip. The laser beam enters at the bottom of the chip and is redirected upon hitting the micromirror sidewall of the polymer-filled cavity.

(~ 200 µm) glass (AF-45, index of refraction $n_1$ = 1.526) wafers. The cavity that is formed between the two glass wafers and the micromirror surfaces is filled with a transparent UV curable polymer (Norland Optical Adhesive 65, index of refraction $n_2$ = 1.524) that couples the exciting light into the system. The UV curable polymer is an essential component for efficient optical coupling, minimizing the reflectance losses to less than 5% (see section E). The top glass wafer serves as the functional substrate where TIR takes place, while the bottom one is used to planarize the UV curable polymer. The light beam is weakly focused on the interface where it is totally internally reflected, creating the evanescent field.

The multilayer chip is fabricated using standard bulk micromachining techniques (Fig. 3). One micron of low stress silicon nitride (LSN) is deposited on a {100}-oriented, 500 microns thick, double-polished silicon substrate. The silicon nitride film is photolithographically patterned and the wafer is immersed in a 2:1

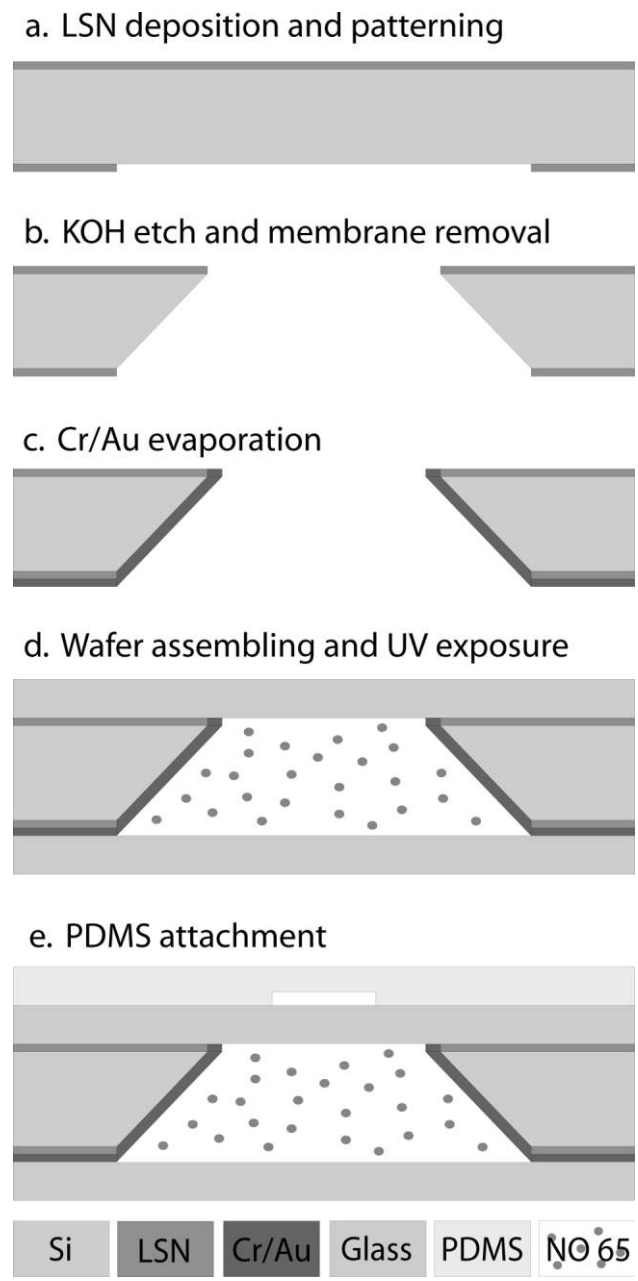


**Fig. 3** The fabrication process of the biochip: (a) low stress silicon nitride (LSN) deposition and patterning, (b) backside KOH etch and front side silicon nitride removal, (c) chrome/gold deposition, (d) wafer assembling through the UV curable polymer and UV blank exposure, (e) PDMS attachment.

KOH solution to obtain the 54.7 ° silicon tilted walls. The suspended nitride membrane that remains at the end of the wet etch process is subsequently broken and removed with a blast of compressed air. A 0.3 μm thick layer of chrome/gold is then electron-beam evaporated to achieve the reflective mirror surface. The silicon substrate is inverted and placed upside-down on the top of the glass substrate. The formed cavity is filled with the UV curable polymer. The bottom glass substrate is placed on top of this assembly, enclosing the cavity. The polymer is fully crosslinked upon UV light exposure for 10 min with a 100 W ultraviolet lamp (Spectroline, SB 100P). This step both cures the polymer in the cavity and bonds all three wafers together. The microfluidic network is formed from a PDMS (polydimethylsiloxane) slab patterned from an SU-8 mold. The mold is created by spin casting and patterning a 13 μm layer of SU-8-2010 on a bare silicon wafer. The PDMS prepolymer mixture is cast over the mold and cured on a hot plate for 15 min at 150° C. After curing, the PDMS replica is peeled off from the mold, treated with oxygen plasma (30 s, 30 W at 1 Torr) and irreversibly attached on top of the top glass substrate to seal the chip.

## D Integrated optical system

A green laser diode (model VLM-532-43LCB from Quarton Inc., optical power output ~5 mW) is used as a fluorescent excitation source. The output light beam is 2 mm in diameter, with linear polarization and a half divergence angle of < 0.3 mrad. Green laser diodes are semiconductor light sources similar to the ones used in green laser pointers with a peak wavelength of 532 nm. They are inexpensive, compact and provide enough optical power to excite fluorescence even when battery operated.

A web CCD camera (QuickCam Pro 4000) is used as a real-time imaging detector. The resolution is limited to 640 × 480 pixels at an adjustable exposure time of 250 ms to 0.1 ms. The web camera is disassembled from its original package and attached to a plastic frame. The recorded images are directly transferred to a computer through a USB port. Although such low-cost CCD cameras are intended for internet videoconferencing, their sensitivity and resolution prove to be adequate for imaging fluorescence too.

The custom-made optical system (Fig. 4) is completed with the addition of a fluorescence filter to suppress the excitation laser light from being detected though the CCD camera and a microscope objective lens. The microscope objective (MicroPlan 40x, Nikon) is separated 3 cm from the camera. A 1 mm pinhole is mounted on the laser head to achieve more uniform illumination. A 25 mm in diameter plano-convex lens with a focal length of 25 mm is also attached at the laser pointer head to weakly focus the beam on the chip surface. The purpose of the focusing lens is to concentrate the laser illumination in much the same manner as an objective during epi-illumination, but to also narrow the beam width so it matches the size of the tilted micromirror surface. The chip is placed on a custom made Plexiglas frame and is positioned 25 mm above the lens–laser setup. The web CCD camera is mounted on a Z-axis manipulator to facilitate focusing. The laser diode is attached on a XYZ-axis manipulator to assist alignment. The whole optical setup extends 28 cm in height.

## E Total internal reflection within the biochip

### Incident angle of illumination and optical coupling efficiency

The incident angle of illumination, $\theta$, in conjunction with the critical angle, $\theta_C$, strongly influence the properties of the evanescent wave and are the most important variables when designing TIRFM configurations. The incident angle can be established by drawing a ray diagram of the light beam as it passes through the biochip (Fig. 2). If the beam is not collimated, the incident angle continuously changes along the focused spot. The inner and outer rays of the beam reach the interface at incident angles of 69.6° and 71.1° respectively, when an AF glass substrate is used and the light is coupled with an UV curable polymer of similar index of refraction (*e.g.* Norland 65). Both values are above the critical angle ($\theta_C$ = 64.8°, for the worst case scenario of $n_2$ = 1.38), so the entire beam is totally internally reflected. As previously described, the initially collimated beam is focused through a lens with a focal length of 25 mm. The distance between the chip and the lens alters only the size of the focused spot and not the incident angle. Depending on the application, larger spots can be obtained if the distance between the lens and the chip is decreased. Such design can be advantageous for the simultaneous excitation of multiple microchannels.

Replacing the Norland 65 polymer with a polymer of different index of refraction (*e.g.* Norland 63 or PDMS with index of refraction equal to 1.56 and 1.41 respectively) modifies the incident angle of illumination at the interface without having to adjust the position of the laser beam. Accounting for all changes in indices of refraction (air to bottom glass substrate to polymer to top glass substrate), the inner and outer rays of the beam can reach the glass/liquid interface at incident angles ranging from 61° to 85° by simply changing the index of refraction of the polymer from 1.41 to 1.61 (Fig. 5). The change in the incident angle of illumination by employing a polymer of different index of refraction demonstrates the flexibility of the employed design to adapt to the needs of a specific application.

Utilization of the UV curable polymer provides high optical coupling efficiency, since it significantly minimizes light losses. If no polymer is incorporated, there is a substantial percentage of light reflected at the air/top glass interface because of the large change in the indices of refraction and the large incident angle. The parallel

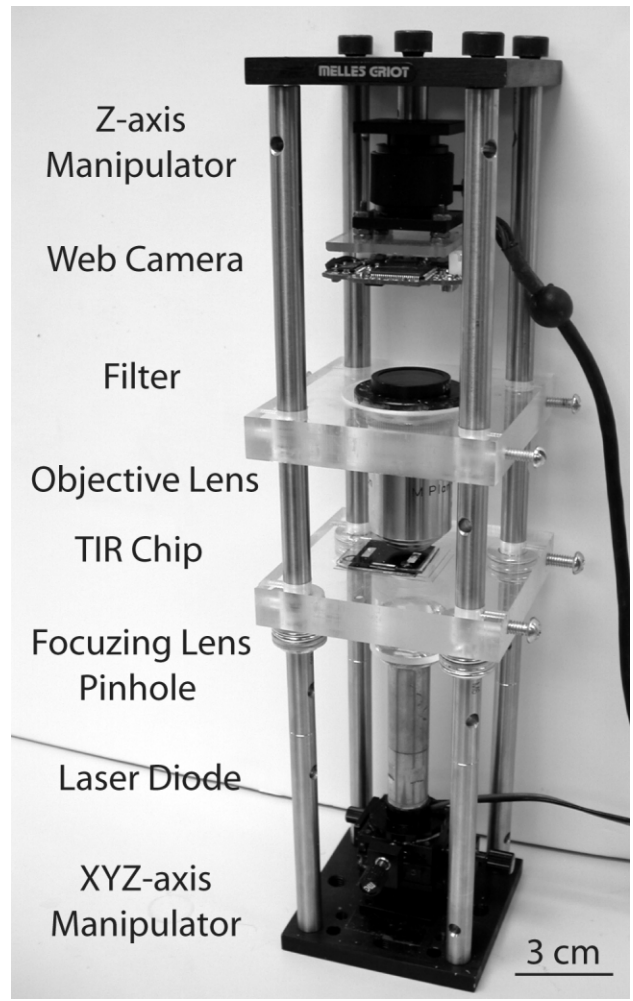


**Fig. 4** The integrated optical system. All the optical components are vertically integrated resulting in a compact system 28 cm in height.

(to the plane of incident) and perpendicular components of the reflectivity losses as a function of incident angle at the bottom of the top glass substrate are depicted in Fig. 6.

The use of Norland 65 reduces the reflectance light losses to 5% of the incident light. If no coupling material is implemented (air/glass interface) the light losses are as high as 35%.

### Evanescent field

A quantitative analysis of the properties of the evanescent field created by the four-layer chip is important in evaluating the range of operation, as well as the limitations of such a configuration, since the emitted fluorescence intensity depends greatly on the s-polarized and p-polarized components of the intensity of the evanescent wave.[11]

Fig. 7, calculated from eqn. (2), depicts graphically the dependence of $I_P(0)$ and $I_S(0)$ on the incident angle of illumination for the implemented geometry and materials (AF glass, Norland 65, $n_2$ = 1.38, $\theta_C$ = 64.81°). For simplicity the s-polarized and p-polarized incident amplitudes ($A_S$ and $A_P$) at the interface are assumed to be unity. Large incident angles significantly reduce the evanescent intensities, $I_P(0)$ and $I_S(0)$, decreasing the probability of energy absorption by a fluorophore. The shadowed area corresponds to all the rays with incident angles between the inner and outer rays. The intensity along the focused spot is therefore exponentially decreasing due to the continuous change of the incident angle.

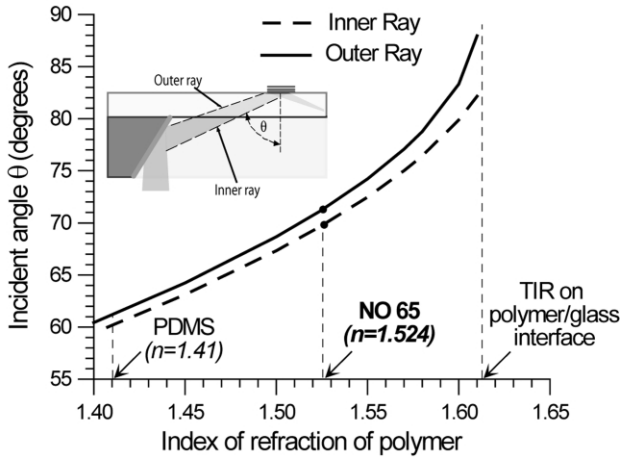


**Fig. 5** Dependence of the incident angle of illumination on the index of refraction of the UV curable polymer. Optical adhesive Norland 65 (NO 65) results in an incident angle of ~70°. PDMS would decrease the incident angle to ~61°.

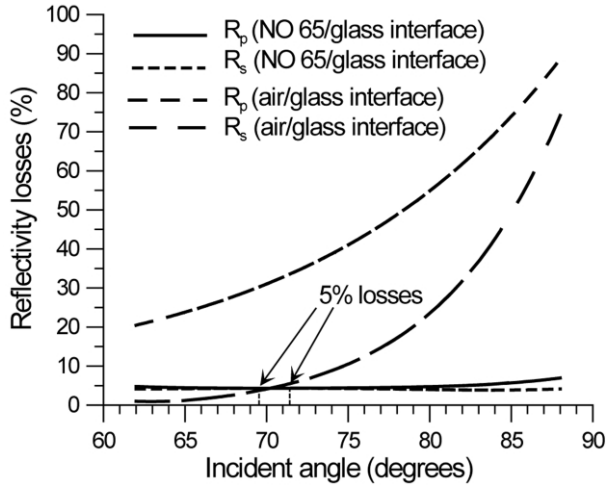


**Fig. 6** Reflection losses at the air/glass and Norland 65/glass interface *versus* incident angle (the subscripts *p* and *s* denote components parallel and perpendicular to the plane of incidence respectively).

For supercritical angles within 10° of the $\theta_C$, the evanescent intensity is generally as great as or greater than the incident light intensity.[5] Because the operation range of incident angles (69.6° < $\theta$ < 71.1°) of our chip is within 10° of the critical angle, the intensity evanescent wave is enhanced at the interface ~3 times of that of the incident light. If it is desired to have uniform illumination, the beam should be collimated so a fixed incident angle is obtained. The above results illustrate that the proposed chip design functions at a range close to the critical angle which is necessary to produce an evanescent field strong enough to excite fluorescence.

## F Experimental results

The ability of total internal reflection fluorescent microscopy (TIRM) to detect real-time events has recently drawn the interest of researchers for studying the dynamics of various biological systems.[13] The ability of our system to perform similar functions is experimentally demonstrated by detecting the Brownian motion of fluorescent microspheres.

We observe the movement of 1 μm diameter nile red fluorescent carboxylate-modified microspheres (Molecular Probes Inc.), suspended in DI water at room temperature. These microspheres have an emission maximum at 575 nm upon excitation by green light (absorption maximum at 535 nm). An interference filter (Optical Omega, XF3021) is used to block green fringing light from the laser source.

After a droplet of the suspension had been pipetted on the chip, a few seconds are needed for the spheres to settle to the glass surface. Microspheres that are permanently adsorbed to the chip fluoresce continuously, while active microspheres that enter and leave the evanescent field due to random Brownian motion are imaged as blinking spots. The continuous Brownian motion of free particles can be verified by observing them with a light microscope.

Fig. 8 shows a sequence of video frames of the motion of a single microsphere (exposure time was set to 33 ms). The sphere is shown to slowly move away and separate (Fig. 8b) from a neighboring sphere that is attached to the substrate. After separation, the microsphere starts moving out of plane, gradually leaving the evanescent field (Fig. 8c) – reduced intensity is observed – until it finally exits the field where no fluorescence signal is observed (Fig. 8d). Several microspheres stuck together and adsorbed to the chip surface are visualized as a fluorescent spot of larger dimensions.

The two dimensional intensity profile of the TIR region can be imaged by depositing rhodamine 6G (R6G) inside the microfluidic network (Fig. 9). Positively charged rhodamine molecules were precipitated on the negatively charged glass surface of the

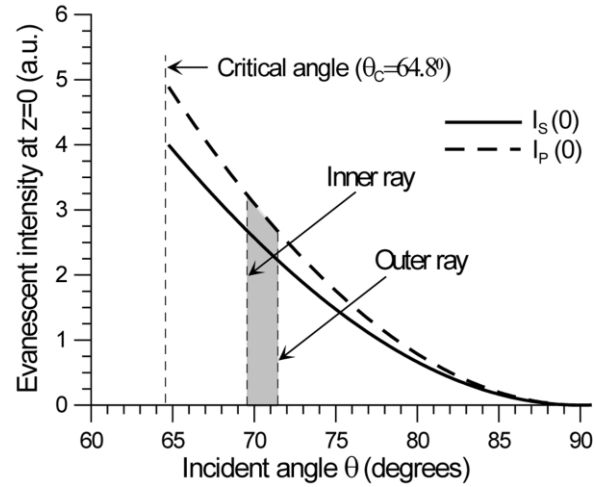


**Fig. 7** Intensity of the evanescent wave at the interface *versus* incident angle. The chip operates at a range of incident angles within 5–7 degrees of the critical angle.

microfluidic channel by evaporating 10 μL of 10 pM concentration of R6G in methanol.

In a similar experiment, we injected 10 μL of 10 fM and 500 fM concentration of R6G that corresponds to 60 230 rhodamine molecules. After complete evaporation (typically after 1–2 min), rhodamine fluorescence intensity was recorded. All the experiments were performed in a dark room. The output optical power of the laser was 2.6 mW (measured with an optical power meter, Newport 1830-C). The normalized fluorescent intensity curves for 10 fM and 500 fM concentrations (Fig. 10) are consistent, yielding a photobleaching rate constant in air of 0.22 $s^{-1}$ and 0.18 $s^{-1}$ respectively. To measure the fluorescent intensity, image processing software (Scion Image) was used to determine the average intensity (per pixel) of a 25 × 15 pixel region within the TIR spot. The background was measured similarly on a 25 × 15 pixel region outside the TIR spot and subtracted from the average fluorescent intensity. Typical signal to background ratios (SBRs) at $t = 0$ were 13.4 and 7.9 for 500 fM and 10 fM respectively. The exposure time was 67 ms. Due to limited dynamic range of the web camera, higher concentrations were not possible to be quantified due to signal saturation.

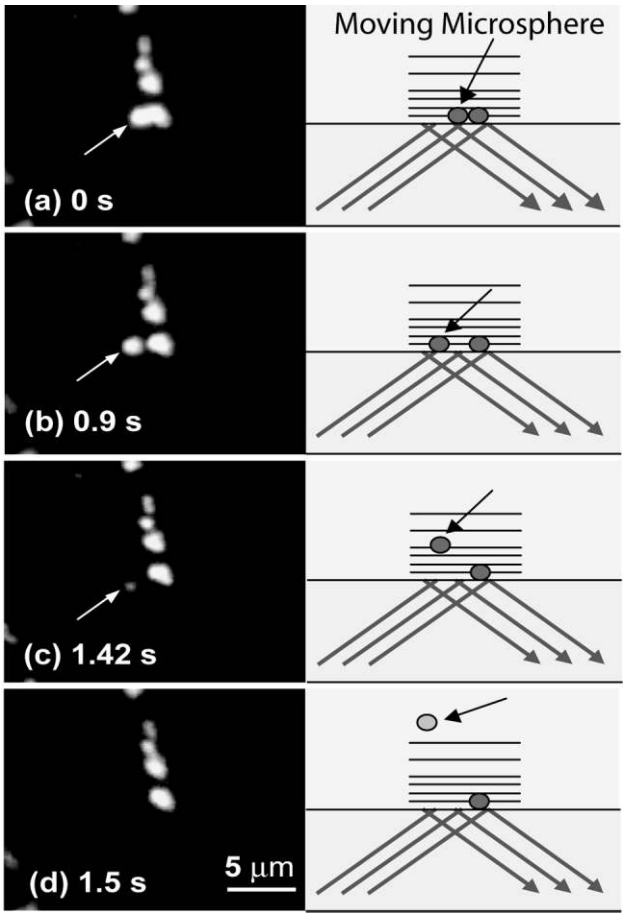


**Fig. 8** Recording the Brownian motion of a single 1 μm fluorescent microsphere.

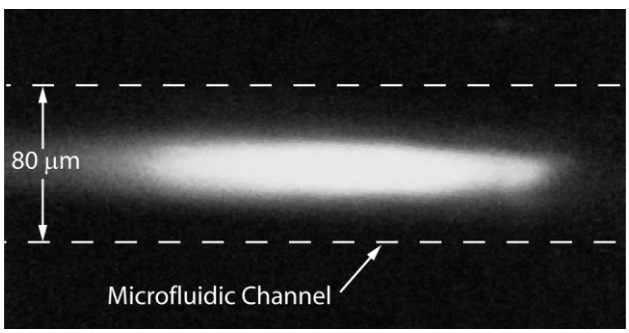


**Fig. 9** Intensity profile of the TIR region in air as visualized upon coating the bottom of the microfluidic channel with rhodamine 6G.

Methanol evaporation starts at the inlet and outlet of the microfluidic network. Consequently, the bulk of rhodamine molecules in solution are carried towards the TIR region where the evaporation is completed (the TIR region is located in the middle of the microfluidic network). For this reason a large fraction of the original number of molecules in solution are deposited close to the TIR region. Due to the uncertainty of the number of molecules deposited on the TIR region, an estimate of the actual number of molecules that were detected was not possible.

We also tried to capture the photobleaching of rhodamine molecules before the microchannel dries, but it was difficult to quantify the results. In filled microchannels, rhodamine molecules accumulate over time on the glass surface while previously precipitated ones are being photobleached. We thus chose to measure the fluorescent intensity in dry environment where the number of molecules adsorbed on the surface is fixed.

To achieve higher sensitivity, the web camera is the first component that needs to be replaced. Intensified video cameras and back-illuminated CCD sensors are at present the best option, providing excellent quantum efficiency, but are ~2000 times more expensive than a web CCD camera. Special care must also be taken for minimizing the autofluorescence of the glass substrate. Quartz has the lowest level of fluorescent impurities and is therefore the material of choice (in our experiments we used AF-75 glass). Background autofluorescence from the UV curable polymer also decreases the signal to noise ratio, but no experimental data are currently available for determining the most appropriate polymer.

## G Conclusions

An optical configuration for generating total internal reflection is proposed using a microfabricated biochip containing a polymer-filled cavity with a micromirror sidewall. Efficient optical coupling is achieved through the use of a UV curable polymer that fills the silicon micromirror cavity. Such a design enables the hybrid vertical integration of all needed elements for an autonomous miniaturized system, eliminating the need for precise alignment of the excitation light into the system. The incident angle is defined by the fabrication process of the fixed silicon micromirror and the index of refraction of the UV curable polymer. Real time detection of the Brownian motion of fluorescent microspheres and photobleaching curves of rhodamine 6G were recorded using a custom-made, compact optical setup consisting of an inexpensive green laser diode and a web CCD camera. Alternatively, the proposed TIR-chip can be easily used with any commercial inverted or

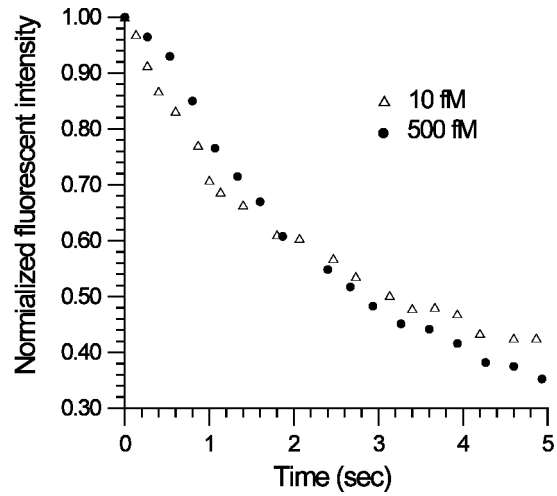


**Fig. 10** Normalized photobleaching curves for rhodamine 6G. After 5 s the signal is reduced to 35% of the initial value. The exposure time was 67 ms.

upright microscope. The end-user need only align a laser diode beneath the TIR-chip. An external focusing lens can also be used if a highly focused TIR spot is desired.

## Acknowledgements

This work is fully supported by a DARPA grant under the BioFlips program. We also acknowledge Jennifer Chen for her assistance with the ray optics results.

## References

1 T. Vo-Dinh and B. Cullum, *Fresenius' J. Anal. Chem.*, 2000, **366**, 540.
2 M. A. Osborne, C. L. Barnes, S. Balasubramanian and D. Klenerman, *J. Phys. Chem. B*, 2001, **105**(15), 3120.
3 C. Peter, M. Meusel, F. Grawe, A. Katerkamp, K. Cammann and T. Borchers, *Fresenius' J. Anal. Chem.*, 2001, **371**(no.2), 120.
4 T. Funatsu, Y. Harada, M. Tokunaga, K. Saito and T. Yanagida, *Nature*, 1995, **374**(no.6522), 555.
5 D. Axelrod and Review, *Traffic*, 2001, **2**, 764.
6 K. Schult, A. Katerkamp, D. Trau, F. Grawe, K. Gammann and M. Meusel, *Anal. Chem.*, 1999, **71**, 5430.
7 H. P. Kao, N. Yang and J. S. Schoeniger, *J. Opt. Soc. Am. A*, 1998, **A15**, 2163.
8 L. Eldada, Xu. Chengzeng, K. M. T. Stengel, L. W. Shacklette and J. T. Yardley, *J. Lightwave Technol.*, 1996, **14**(7), 1704.
9 G. L. Duveneck, M. Pawlak, D. Neuschafer, E. Bar, W. Budach, U. Pieles and M. Ehrat, *Sens. Actuators B*, 1997, **B38**(no.1–3), 88.
10 W. Budach, A. P. Abel, A. E. Bruno and D. Neuschafer, *Anal. Chem.*, 1999, **71**(16), 3347.
11 D. Axelrod, E. H. Hellen and R. M. Fullbright, *Topics in fluorescence spectroscopy*, 1992, **3**: **biochemical applications**, New York: Plenum Press, 289.
12 A. Tronin and J. K. Blasie, *Langmuir*, 2001, **17**, 3696.
13 D. W. Pierce, N. Hom-Booher and R. D. Vale, *Nature*, 1997, **388**, 3.